

# New Bismuth-Substituted Hydroxyapatite Nanoparticles for Bone Tissue Engineering

GABRIELA CIOBANU,<sup>1,2</sup> ANA MARIA BARGAN,<sup>1</sup>  
and CONSTANTIN LUCA<sup>1</sup>

1.—Faculty of Chemical Engineering and Environmental Protection, “Gheorghe Asachi” Technical University of Iasi, Prof. Dr. Docent Dimitrie Mangeron Rd., No. 63, 700050 Iasi, Romania.  
2.—e-mail: gciobanu03@yahoo.co.uk

New bismuth-substituted hydroxyapatite  $[\text{Ca}_{10-x}\text{Bi}_x(\text{PO}_4)_6(\text{OH})_2]$  where  $x = 0\text{--}2.5$  nanoparticles were synthesized by the co-precipitation method from aqueous solutions. The structural properties of the samples were analyzed by scanning electron microscopy coupled with x-ray analysis, x-ray powder diffraction, x-ray photoelectron spectroscopy, Fourier transform infrared spectroscopy and Brunauer–Emmett–Teller surface area analysis. The results confirm that bismuth ions have been incorporated into the hydroxyapatite lattice. The prepared nanocrystalline powders consisted of hydroxyapatite as single phase with hexagonal structure, crystal sizes smaller than 60 nm and (Bi + Ca)/P atomic ratio of around 1.67. The hydroxyapatite samples doped with Bi have mesoporous textures with pores size of around 2 nm and specific surface area in the range of 12–25 m<sup>2</sup>/g. The Bi-substituted hydroxyapatite powders are more effective against Gram-negative *Escherichia coli* bacteria than Gram-positive *Staphylococcus aureus* bacteria.

## INTRODUCTION

Hydroxyapatite [HAp,  $\text{Ca}_{10}(\text{PO}_4)_6(\text{OH})_2$ ] is a calcium phosphate ceramic with important applications in the medicine and chemistry fields and is a main mineral constituent of hard tissues such as bones and teeth.<sup>1</sup> Hydroxyapatite has remarkable properties including biocompatibility, bioactivity and ability to form a direct chemical bond with human hard tissues.<sup>2–4</sup>

The hydroxyapatite structure allows the incorporation of wide range of different ionic substitutions.<sup>5</sup> Numerous monovalent ( $\text{Na}^+$ ,  $\text{K}^+$ ), divalent ( $\text{Sr}^{2+}$ ,  $\text{Pb}^{2+}$ ,  $\text{Ba}^{2+}$ ,  $\text{Mn}^{2+}$ ,  $\text{Cd}^{2+}$ ,  $\text{Mg}^{2+}$ , etc.), trivalent ( $\text{Cr}^{3+}$ ,  $\text{Al}^{3+}$ ,  $\text{Fe}^{3+}$ , rare earths ions  $\text{REE}^{3+}$ , etc.), tetravalent ( $\text{Ti}^{4+}$ ,  $\text{Th}^{4+}$ ,  $\text{U}^{4+}$ ) and even hexavalent ( $\text{U}^{6+}$ ) cations have been reported to substitute into the Ca sites in the hydroxyapatite structure.<sup>6–9</sup> Such ionic substitutions influence the properties (morphology, lattice parameters, surface characteristic, solubility, mechanical and biological properties) and applications of these doped hydroxyapatite materials as biomaterials, catalysts, ion exchangers, etc.<sup>10,11</sup>

For more than a century, the bismuth salts have been used as a remedy for some maladies such as gastrointestinal disorders, syphilis and hypertension.<sup>12</sup> Today, the two major medicinal uses of bismuth are as an antimicrobial agent and N anticancer agent.<sup>13</sup> Bismuth compounds, due to their radio-opacity, are also added to various bone and dental implants, catheters and surgical instruments in order to make them detectable by x-rays and computed tomography.<sup>14,15</sup>

In the available literature, only a few studies are devoted to calcium phosphates (as dicalcium or tetracalcium phosphates) doped with bismuth ions,<sup>16</sup> while the  $\text{Ca}^{2+}$  substitution with  $\text{Bi}^{3+}$  ions in a hydroxyapatite lattice has not previously been studied in detail. Therefore, in this paper, we present the preparation of new bismuth-substituted hydroxyapatite nanopowders by means of the wet chemical method, by co-precipitation reactions. The effects of the bismuth substitution for calcium on the morphology, purity, crystallinity, crystallite size and antibacterial activity of the resulting bismuth-substituted hydroxyapatite powders were investigated and discussed.

## EXPERIMENTAL

### Materials and Synthesizing Methods

Calcium hydroxide  $\text{Ca}(\text{OH})_2$ , orthophosphoric acid  $\text{H}_3\text{PO}_4$  (85%), bismuth nitrate pentahydrate  $\text{Bi}(\text{NO}_3)_3 \cdot 5\text{H}_2\text{O}$ , ethanol  $\text{CH}_3\text{-CH}_2\text{-OH}$  and sodium hydroxide  $\text{NaOH}$  were purchased from Sigma-Aldrich (Germany). All chemicals were of analytical grade.

Hydroxyapatite and bismuth-substituted hydroxyapatite nanoparticles with various Bi content (0–25%) were synthesized by the wet chemical precipitation method from  $\text{Ca}(\text{OH})_2$ ,  $\text{H}_3\text{PO}_4$  and  $\text{Bi}(\text{NO}_3)_3 \cdot 5\text{H}_2\text{O}$  as calcium, phosphorous and bismuth sources, respectively.

Pure hydroxyapatite powder was prepared by adding drop-wise 250 mL of  $\text{Ca}(\text{OH})_2$  (0.1 M) aqueous solution to an appropriate amount of  $\text{H}_3\text{PO}_4$  (0.1 M) aqueous solution to achieve the predetermined Ca/P atomic ratio of 1.67, under magnetic stirring for 1 h. The pH was continuously monitored and adjusted to  $11 \pm 0.5$  by adding  $\text{NaOH}$  (1 M). The suspension was aged for 3 h and then filtered and washed with ethanol and triply distilled water. The obtained powder was calcined 1 h at  $800^\circ\text{C}$  in an electrically heated furnace in order to increase its crystallinity.

The bismuth-substituted hydroxyapatite powders of different compositions were prepared similarly to the pure hydroxyapatite powder, as described above. The  $\text{Ca}(\text{OH})_2$  (0.1 M) aqueous solution was dispersed into an mixed aqueous solution of  $\text{Bi}(\text{NO}_3)_3 \cdot 5\text{H}_2\text{O}$  and  $\text{H}_3\text{PO}_4$  (0.1 M). The (Bi + Ca)/P atomic ratio was kept at 1.67, while the Bi/(Bi + Ca) atomic ratio (denoted as  $X_{\text{Bi}}$ ) in the solution varied between 0.01 and 0.25, as shown in Table I. The following procedure stages were the same as described above for the preparation of pure hydroxyapatite powder.

### Characterization of Samples

Calcium hydroxide  $\text{Ca}(\text{OH})_2$ , orthophosphoric acid  $\text{H}_3\text{PO}_4$  (85%), bismuth nitrate pentahydrate  $\text{Bi}(\text{NO}_3)_3 \cdot 5\text{H}_2\text{O}$ , ethanol  $\text{CH}_3\text{-CH}_2\text{-OH}$  and sodium hydroxide  $\text{NaOH}$  were purchased from Sigma-Aldrich (Germany). All chemicals were of analytical grade.

The phase composition, degree of crystallinity and size of crystallites of the calcined samples were estimated by x-ray diffraction analysis (XRD) with a X'PERT PRO MRD diffractometer using Cu  $K\alpha$  radiation ( $\lambda = 0.15418$  nm). The data were collected in the  $2\theta$  range of  $20^\circ$ – $70^\circ$ , with a step size of  $0.04^\circ$   $2\theta$  and a counting time of 80 s per data point. The lattice parameters  $a$  and  $c$  (nm) for the hexagonal hydroxyapatite structure, were calculated from peaks (002) and (211), respectively, using the following equation:

$$\frac{1}{d^2} = \frac{4}{3} \cdot \left( \frac{h^2 + h \cdot k + k^2}{a^2} \right) + \frac{l^2}{c^2} \quad (1)$$

where  $d$  is the distance (nm) between adjacent planes in the set of Miller indices ( $hkl$ ).

The volume  $V$  ( $\text{nm}^3$ ) of the hexagonal unit cell was calculated using relationship:

$$V = 2.589 \cdot a^2 \cdot c \quad (2)$$

The average crystallite size  $D$  (nm) of the powders was calculated from XRD data using the Scherrer equation:

$$D = \frac{k \cdot \lambda}{B_{1/2} \cdot \cos \theta} \quad (3)$$

where  $\lambda$  is the wavelength of Cu  $K\alpha$  radiation ( $\lambda = 0.15418$  nm),  $B_{1/2}$  is the full width at the half-maximum intensity value for the diffraction peak under consideration (rad),  $\theta$  is the diffraction angle of the corresponding reflection ( $^\circ$ ), and  $k$  is the broadening constant varying with crystal habit and chosen as 0.9 for the hydroxyapatite crystallites. For quantitative determinations, the peak at  $2\theta = 25.9^\circ$  for (002) reflection was used to evaluate the crystallite size of hydroxyapatite powders. It is due to the fact that this peak is well resolved and shows no interferences.

The crystallinity degree  $X_{\text{C}}$  (%) corresponding to the fraction of crystalline phase of the hydroxyapatite powders was evaluated by the equation:

$$X_{\text{C}} = \frac{I_{300} - V_{112/300}}{I_{300}} \cdot 100 \quad (4)$$

where  $I_{300}$  is the intensity of (300) diffraction peak

**Table I. Atomic ratios in the synthesis solution and in the final products**

Sample	In synthesis solution			In final product		
	Bi/(Bi + Ca)	(Bi + Ca)/P	Bi (%)	Bi/(Bi + Ca)	(Bi + Ca)/P	Bi (%)
HA-Bi-0	0	1.677	0	0	1.673	0
HA-Bi-5	0.05	1.677	5	0.0498	1.666	4.98
HA-Bi-10	0.10	1.677	10	0.0933	1.660	9.33
HA-Bi-15	0.15	1.677	15	0.1449	1.671	14.49
HA-Bi-25	0.25	1.677	25	0.2443	1.683	24.43

and  $V_{112/300}$  the intensity of the hollow between the (112) and (300) diffraction peaks of hydroxyapatite.

The morphology of the calcined samples was studied by scanning electron microscopy (SEM) coupled with energy dispersive x-ray spectroscopy (EDX) with QUANTA 200 3D microscope. Gold sputtering was used to make the coating surfaces conductive for the SEM investigations. The bismuth chemical valence on the hydroxyapatite structure was evaluated by x-ray photoelectron spectroscopy (XPS) using a PHI-5000 VersaProbe photoelectron spectrometer ( $\Phi$  ULVAC-PHI) with a hemispherical energy analyzer (0.85 eV binding energy resolution). A monochromatic Al K $\alpha$  x-ray radiation ( $h\nu = 1486.7$  eV) was used as the excitation source. The surface chemical composition of each sample was analyzed using a combination of XPS and SEM/EDX. With these methods, the contents of Ca, P and Bi in the samples have been determined, from which the Ca/P or Bi + Ca/P atomic ratios values were calculated. The FTIR spectra of all samples were taken by the KBr method using a DIGILAB SCIMITAR-SERIES spectrophotometer. The specific surface areas were evaluated by fitting the Brunauer–Emmett–Teller (BET) equation to the N<sub>2</sub> adsorption isotherms recorded by a Quantachrome Nova 2200e Win2 apparatus. The pore size distribution was obtained by Barrett–Joiner–Halenda (BJH) method from the desorption curve of the isotherm.

### Antibacterial Activity

The disc diffusion test method (commonly known as the Kirby–Bauer disc diffusion method) was used to investigate the antibacterial activity of the samples against Gram-positive *Staphylococcus aureus* and Gram-negative *Escherichia coli* bacteria.<sup>17</sup> The bacterial strains were provided by the microbiology laboratory of the “Gheorghe Asachi” Technical University of Iasi, Romania. Mueller–Hinton agar was cast into the Petri plates and the plates containing the nutrient medium were separately inoculated with the test organisms of *Escherichia coli* and *Staphylococcus aureus*. The samples were planted onto the agar plates and then incubated at 37°C for 24 h. The bacterial resistance of the samples was examined for a zone of inhibition and the total diameter (in mm) of the inhibition zone was measured. The microbial inhibition (%) was calculated taking into account the microbial mass of substance which was reported for a 0.5 g sample and inhibition zone diameter. The antibacterial assessment was performed in duplicate and the average results were reported.

## RESULTS AND DISCUSSION

### Substitution Mechanism

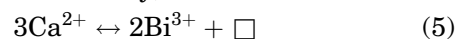
The replacement of Ca<sup>2+</sup> with other cations in the hydroxyapatite crystalline lattice induces changes in the hydroxyapatite properties which may be related to

the ionic radius, electronegativity and effective charge of the substituting cation compared to those of Ca<sup>2+</sup>. Suzuki<sup>18</sup> studied hydroxyapatite as an inorganic cation exchangers and drawn the conclusion that the cations are more likely to be removed by hydroxyapatite when they have high electronegativity values and radii within the 0.9–1.3 Å range.

The crystallographic structure of hydroxyapatite plays a major role in the substitution of foreign ions in the apatite lattice. The crystal structure of hydroxyapatite is hexagonal with the  $P6_3/m$  space group and the lattice parameters of  $a = b = 9.424$  Å and  $c = 6.879$  Å.<sup>19</sup> The hydroxyapatite lattice comprises two calcium atoms with different crystal configurations, denoted Ca(1) and Ca(2). The Ca(1) atoms are nine-fold coordinated and they occupy the columnar sites. The Ca(2) atoms are seven-fold coordinated and are located in the channels that pass through the three-dimensional network of the PO<sub>4</sub> tetrahedra. The hydroxyapatite structure comprises about 40% of calcium atoms in Ca(1) position and about 60% in the Ca(2) position.<sup>20</sup> The two Ca positions in apatite offer quite different stereochemical environments and are able to accommodate a variety of cations as substituents. Theoretically, it could be thought that the foreign ions larger than Ca<sup>2+</sup> would substitute primarily in the Ca(1) sites while smaller ones would preferentially substitute for Ca(2). Some investigations on substitutions in calcium hydroxyapatite have also shown that the site preference of the substituent cation depends on its effective charge. It was found that the ion with a charge smaller than a charge of calcium mostly occupies the larger Ca(1) site, whereas the ion with a greater charge occupies the more compact Ca(2) site.<sup>21</sup>

The incorporation of Bi<sup>3+</sup> ions in the hydroxyapatite structure is favorable when the difference between the ionic radii is small, close to the ionic radius of Ca<sup>2+</sup> ion. According to Shannon,<sup>22</sup> the effective Ca<sup>2+</sup> ionic radii for seven- and nine-coordinations are of 1.06 Å and 1.18 Å, respectively. For Bi<sup>3+</sup>, the ionic radii are of 1.03 Å and 1.17 Å in six- and eight-coordinations, respectively. Having comparable dimensions, the Bi<sup>3+</sup> ions can substitute Ca<sup>2+</sup> ions during the synthesizing process.

Likewise, because the Bi<sup>3+</sup> ion has greater positive charge than Ca<sup>2+</sup>, a coupled substitution is necessary to maintain charge balance. Several studies have indicated that trivalent cations can substitute for Ca via a Ca-deficiency mechanism such as vacancies.<sup>23</sup> The calcium vacancies formation is the most likely mechanism for compensation of excess positive charge of Bi<sup>3+</sup> ions in the Ca sites. So, the local charge compensation in the Bi-doped hydroxyapatite may be maintained by the following coupled substitution ( $\square$  represents calcium vacancy):



Considering the above, the present study is aimed at obtaining and characterizing the hydroxyapatite substituted with bismuth. By performing XRD,

SEM-EDX and XPS analysis, we wanted to demonstrate that  $\text{Bi}^{3+}$  ions are present in the apatite lattice.

### Chemical Composition

The SEM-EDX analysis was performed in order to determine the surface elemental composition of the hydroxyapatite and Bi-substituted hydroxyapatite powders. Figure 1 shows the EDX spectra of HA-Bi-0 and HA-Bi-25 samples, and for the latter the characteristic peaks of bismuth are well evidenced. All the samples contain calcium or/and bismuth, phosphorous, oxygen and hydrogen in certain contents. The mass fractions of different elements in the hydroxyapatite and Bi-substituted hydroxyapatite samples were obtained and the atomic ratios calculated as shown in Table I.

The values of the  $\text{Bi}/(\text{Bi} + \text{Ca})$  atomic ratio (designated  $X_{\text{Bi}}$ ) in the final products were very close to the  $X_{\text{Bi}}$  in the synthesis solution for all Bi-substituted hydroxyapatite samples, as shown in Table I. The bismuth content in the Bi-substituted hydroxyapatite samples increases with the increasing bismuth concentrations in the precursor solutions. These results indicate that bismuth ions added to the synthesis solution are incorporated into the hydroxyapatite lattice. Furthermore, the values of the  $(\text{Bi} + \text{Ca})/\text{P}$  atomic ratio in the final products (Table I) were very close to the theoretical value of 1.677 for the stoichiometric hydroxyapatite.<sup>20</sup> This result indicates that the isomorphous substitution  $\text{Ca} \leftrightarrow \text{Bi}$  does not significantly affect the stoichiometry of the Bi-substituted hydroxyapatite samples.

### Crystal Morphology

All apatite samples exhibit nanosized spherical shapes and agglomeration with intergranular micropores, as shown in the SEM micrographs in Fig. 2. The Bi content in apatite does not result in strong changes in morphology but in greater

agglomeration. A possible explanation of the agglomeration behavior is the dominating surface properties associated with nanosized crystallites, which causes them to clump together, as observed in Fig. 2. When samples are calcined at high temperature ( $800^\circ\text{C}$ ) in order to increase their thermal and chemical stability, the particles tend to sinter into agglomerates.<sup>24</sup> All the samples exhibit the same morphology. The SEM images reveal a decrease of the particles size from about 51 nm (HA-Bi-0 sample) to 28 nm (HA-Bi-25 sample) with increasing Bi content, in agreement with the XRD data.

In terms of optical properties, the uncalcined samples were white (Fig. 3). The color of the samples was affected by their calcination at  $800^\circ\text{C}$ . Thus, the pure hydroxyapatite (HA-Bi-0 sample) appeared blue in color whereas a yellow color was observed for Bi-substituted hydroxyapatite samples, suggesting the presence of  $\text{Bi}^{3+}$  cations (in the state  $f^0$ , yellow) (Fig. 3). Their color intensities varied proportionally with the doping concentrations. These optical observations can be correlated with the corresponding XPS results which revealed that the  $\text{Bi}^{3+}$  cations (in the state  $f^0$ , yellow) exist at the surface of the samples.

### Crystal Structure

The phase composition, lattice parameters, degree of crystallinity and size of crystallites of the samples were determined by XRD analysis and the obtained results are shown in Fig. 4 and Table II. The XRD patterns in Fig. 4 are in good agreement with the hexagonal (space group P63/m) hydroxyapatite phase (JCPDS Data Card 09-0432) and none of the patterns displayed extra peaks, indicating that all the samples were single phase hydroxyapatite. Compared with pure hydroxyapatite, all the Bi-substituted hydroxyapatite samples showed comparable peaks without significant shifting of the peak positions, regardless of

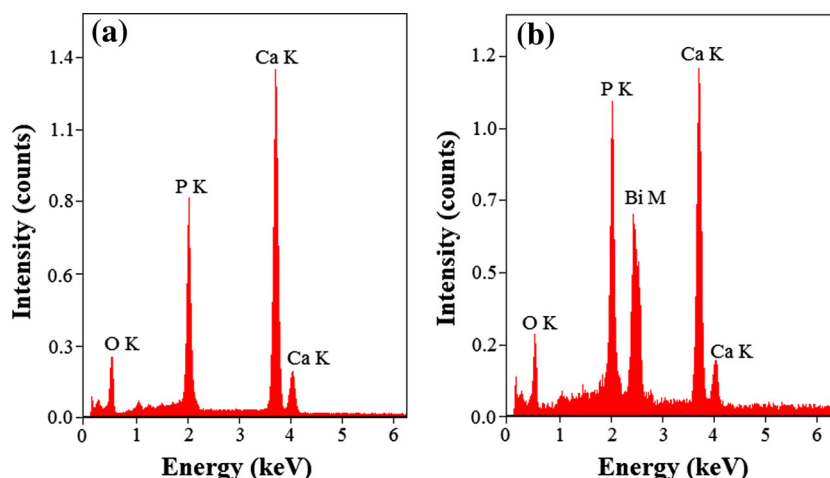


Fig. 1. EDX spectra of the HA-Bi-0 (a) and HA-Bi-25 (b) calcined samples.



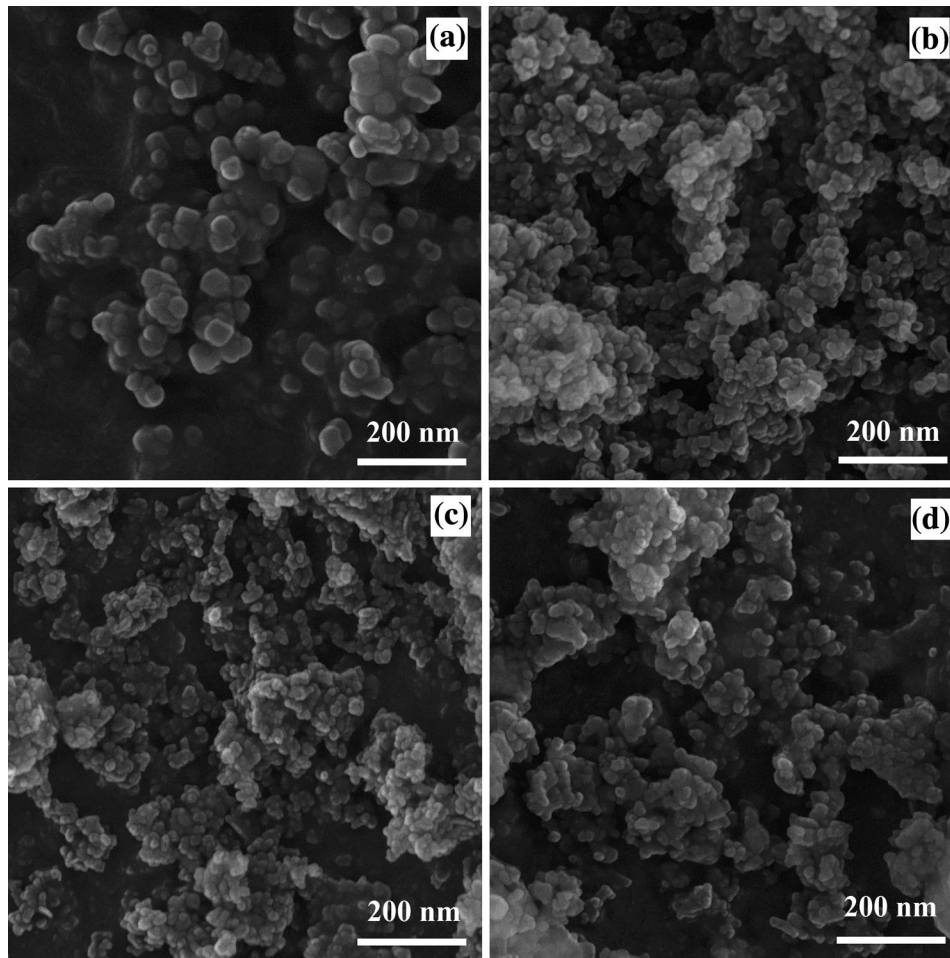


Fig. 2. SEM images of the HA-Bi-0 (a), HA-Bi-5 (b), HA-Bi-15 (c) and HA-Bi-25 (d) samples.

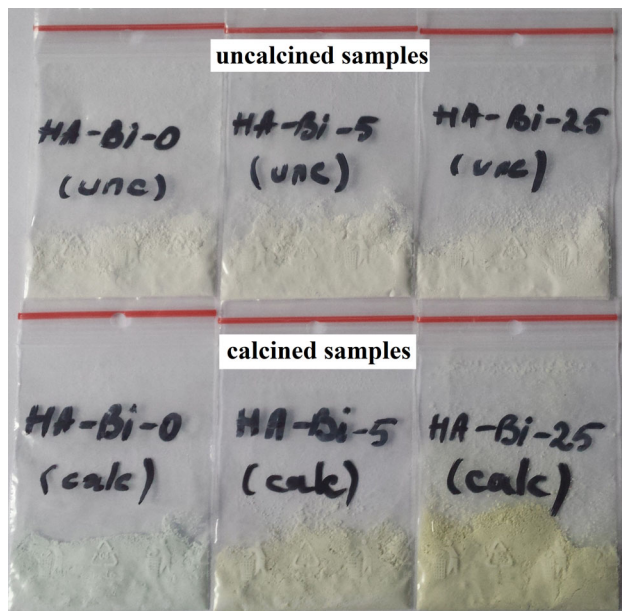


Fig. 3. Optical images of the uncalcined and calcined hydroxyapatite samples.

the substitution concentrations. This suggested that the ion exchange process did not greatly modify the structure of the hydroxyapatite.

The XRD patterns of the Bi-substituted hydroxyapatite samples show the peaks to be broader and less intense compared with the pure hydroxyapatite (HA-Bi-0 sample). This indicates the decrease of crystallinity with increasing bismuth contents (Table II), which could be attributed to a different charge compensation mechanism for isomorphous substitution of  $\text{Ca}^{2+}$  by  $\text{Bi}^{3+}$  ions. The decreased crystallinity of the Bi-substituted hydroxyapatite samples might further lead to increased solubility, thus contributing to the local release of bismuth ions which may in turn improve the biodegradability and antibacterial properties.<sup>16</sup>

Also, the broad peaks indicated that the hydroxyapatite particles are of a nanometric size. The average crystallite size of the pure hydroxyapatite (HA-Bi-0 sample) estimated using the Scherrer equation was 58.32 nm and for the Bi-substituted hydroxyapatite powders was smaller than 51 nm (Table II). For all the samples doped with Bi, a decrease in crystallite size with increasing Bi con-

tent was observed, in agreement with the SEM images.

The lattice parameters  $a$  and  $c$  were obtained from the XRD peaks corresponding to the (002) and (211) planes, which are well resolved and show no interferences. In the case of the substitution of  $\text{Bi}^{3+}$  into the apatite structure, due to the similarities between the ionic radii of  $\text{Ca}^{2+}$  and  $\text{Bi}^{3+}$  no changes in the lattice are expected, although the difference in valence caused by this substitution requires an increase in anionic charge to maintain charge balance. This is achieved through the formation of calcium vacancies on the cation sites. As can be seen in Table II, the lattice parameters and crystal volume of the Bi-substituted hydroxyapatite samples are very close to those of pure hydroxyapatite. However, a slow increase in lattice parameters and crystal volume with increasing Bi content was observed.

### XPS Analysis

The XPS analysis was applied to study the surface chemical state of undoped and Bi-substituted hydroxyapatite and the results present the evidence for the successful doping of Bi ions in the hydroxyapatite lattice. Thus, Fig. 5 shows the XPS spectrum of the HA-Bi-25 sample for the binding

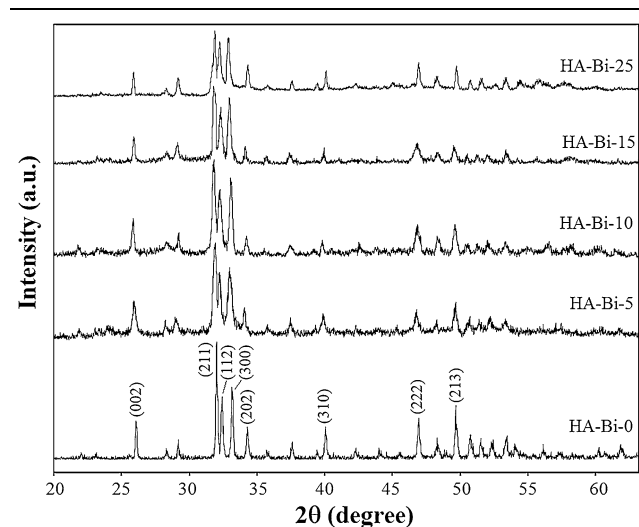


Fig. 4. XRD patterns of the hydroxyapatite and Bi-substituted hydroxyapatite samples.

energy range of 0–1200 eV. It can be seen that the binding energy of Bi (4*f* region, 150–170 eV; peaks at 156.70 eV and 162 eV), Ca (2*p*, 345 eV), O (1*s*, 529 eV) and P (2*p*, 131 eV) were detected. The P 2*p* core level peak located at 131 eV is attributed to P-O bonds in the  $\text{PO}_4^{3-}$  chemical environment.<sup>25</sup> The C 1*s* (282.7 eV) signal is due to the carbon used as an internal reference. No other impurities were evident in the samples, in good agreement with the XRD data. Therefore, the XPS data demonstrate that the HAp lattice contains  $\text{Bi}^{3+}$  ions.

### Textural Characterization and Surface Properties

The surface properties of the Bi-substituted hydroxyapatite samples were determined by fitting the BET equation to the  $\text{N}_2$  adsorption isotherms. Figure 6 shows the nitrogen adsorption isotherms and pore size distribution (inset) of the HA-Bi-0 as well as HA-Bi-25 nanopowders calcined at 800°C. Similar results were obtained for all the samples, and the textural parameters of the corresponding materials are summarized in Table III.

According to the IUPAC classification, all the samples show similar VI isotherms and typical H1-hysteresis loops, demonstrating properties of mesoporous materials. The BJH pore size distribution indicates a micro- (pore diameter < 2 nm) and me-

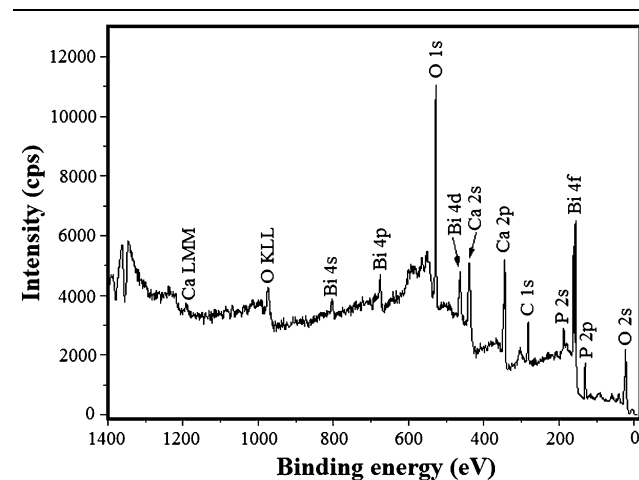


Fig. 5. XPS spectrum of the HA-Bi-25 sample.

**Table II. Crystallites size ( $D$ ), degree of crystallinity ( $X_C$ ), unit cell volume ( $V$ ) and lattice parameters ( $a$  and  $c$ ) of the hydroxyapatite and Bi-substituted hydroxyapatite samples**

Sample	$D$ (nm)	$X_C$ (%)	$V$ ( $\text{\AA}^3$ )	$a$ ( $\text{\AA}$ )	$c$ ( $\text{\AA}$ )
HA-Bi-0	58.32	99.78	1605.77	9.5271	6.8333
HA-Bi-5	51.01	92.75	1616.90	9.5297	6.8769
HA-Bi-10	44.19	90.97	1627.17	9.5514	6.8892
HA-Bi-15	42.60	88.95	1629.46	9.5597	6.8869
HA-Bi-25	36.02	84.16	1632.34	9.5623	6.8953

soporous (pore of 2–12 nm) texture for all samples. The results reveal that the doping of Bi ions has not altered the basic pore structure of the mesoporous hydroxyapatite. The BET surface area correlates well with  $X_{\text{Bi}}$  atomic ratios of the doped samples. A decrease in the surface area of the Bi-substituted hydroxyapatite powders with increasing Bi content was noticed.

## FTIR

The FTIR spectra obtained for pure hydroxyapatite and Bi-substituted hydroxyapatite powders are given in Fig. 7. These spectra provide a number of spectral details demonstrating the formation of hydroxyapatite phase.<sup>20,26</sup> The spectrum of the pure hydroxyapatite (HA-Bi-0) sample shows bands at  $1093\text{ cm}^{-1}$ ,  $1028\text{ cm}^{-1}$  and  $962\text{ cm}^{-1}$  due to the stretching mode of P-O, whereas the bands at  $601\text{ cm}^{-1}$ ,  $567\text{ cm}^{-1}$  and  $472\text{ cm}^{-1}$  are due to the bending mode of O-P-O. The bands at  $2146\text{--}1996\text{ cm}^{-1}$  are attributable to the  $\text{PO}_4^{3-}$  ions. A significant concentration of  $\text{OH}^-$  groups exists in

the apatite structure as observed from the intensity of the bands at  $3572\text{ cm}^{-1}$  and  $632\text{ cm}^{-1}$ . Molecular and adsorbed water bands are also present at  $1654\text{ cm}^{-1}$  and  $3446\text{ cm}^{-1}$  (as a broader band).

The Bi-substituted hydroxyapatite samples show structures similar to pure hydroxyapatite. However, it may be noticed that the peak strengths of the O-H and P-O bonds decrease gradually with the increasing Bi amount in the apatite lattice. Thus, it can be seen that the intensity of the  $3572\text{ cm}^{-1}$  band assigned to the  $\text{OH}^-$  groups decreases without changes in the wavenumber. Therefore, the acidity of the surface P-OH groups was lowered by replacing  $\text{Ca}^{2+}$  with  $\text{Bi}^{3+}$  ions. The weakening of the  $\text{OH}^-$  bands might be caused by the breakage of the electric charge balance in the apatite lattice due to the substitution of  $\text{Ca}^{2+}$  with  $\text{Bi}^{3+}$  ions. In order to compensate these positive charges,  $\text{OH}^-$  might be transformed into  $\text{O}^{2-}$ , as suggested by Serret.<sup>27</sup>

From the FTIR and SEM-EDX, XPS, XRD results, the conclusion can be drawn that the  $\text{Bi}^{3+}$  ions are actually doped into the hydroxyapatite lattice. The experimental results reveal that Bi doping slowly

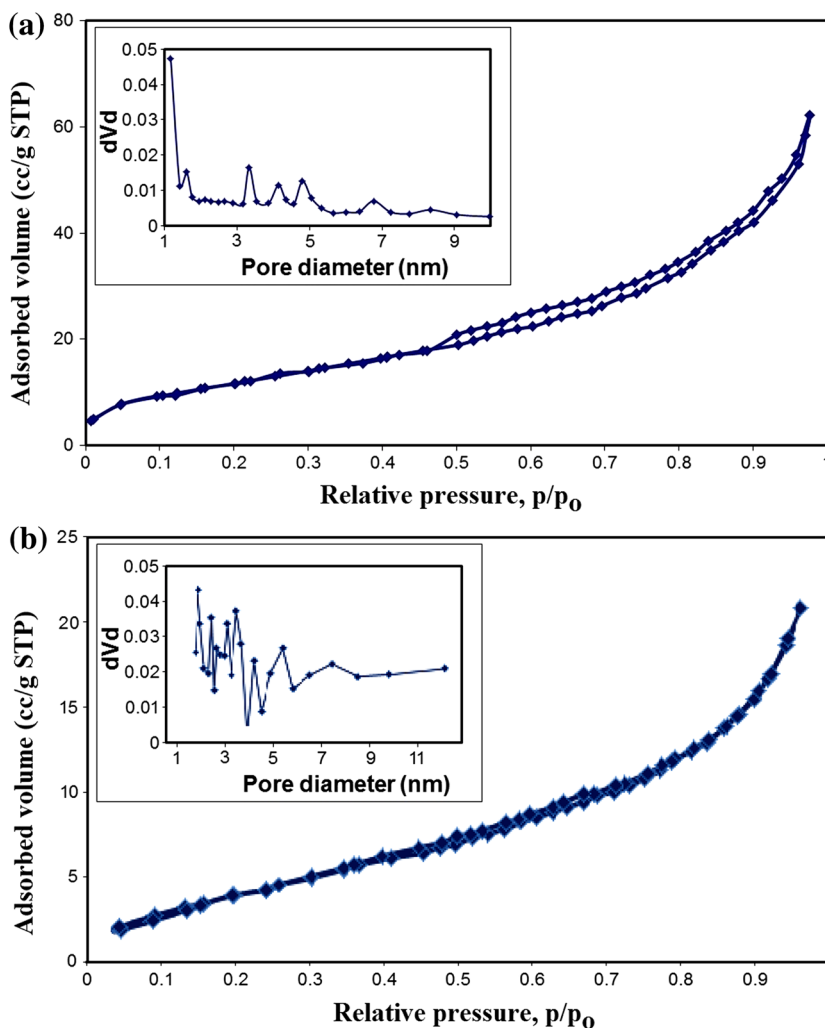


Fig. 6. Adsorption isotherm and pore size distribution (*inset*) of the HA-Bi-0 (a) and HA-Bi-25 (b) samples.

**Table III. Surface properties of the hydroxyapatite and Bi-substituted hydroxyapatite samples**

Sample	Specific surface area (m <sup>2</sup> /g)	External surface area (m <sup>2</sup> /g)	Total pore volume (cm <sup>3</sup> /g)	Average pore size (nm)
HA-Bi-0	139.365	45.454	0.098	1.181
HA-Bi-5	24.866	17.533	0.048	1.645
HA-Bi-10	21.698	14.967	0.041	2.064
HA-Bi-15	20.008	14.423	0.033	1.542
HA-Bi-25	12.030	8.580	0.021	2.180

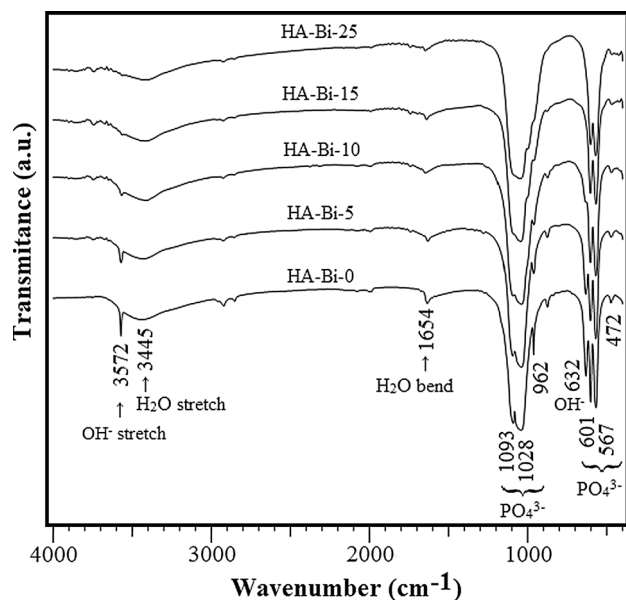
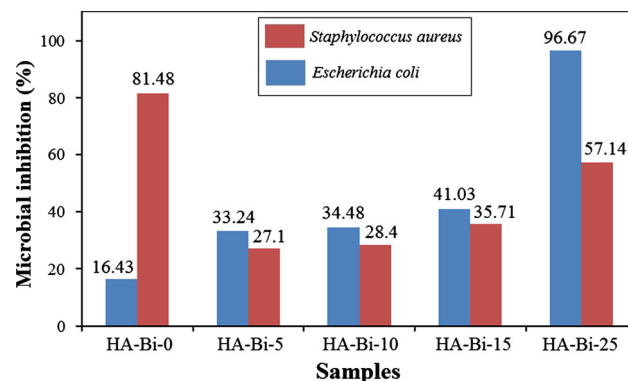


Fig. 7. FTIR spectra of the hydroxyapatite and Bi-substituted hydroxyapatite samples.

affects the hydroxyapatite crystallinity, crystal size, textural and surface properties.

### Antibacterial Activity

In our study, the antibacterial properties of hydroxyapatite and Bi-substituted hydroxyapatite nanopowders were performed through the inhibition zone method against *Escherichia coli* (Gram-negative bacteria) and *Staphylococcus aureus* (Gram-positive bacteria). As revealed in Fig. 8, the level of microbial growth of both bacteria varies differently with increasing Bi amounts in the Bi-doped samples compared to the pure hydroxyapatite sample. The *Escherichia coli* bacterium has a high sensitivity to the samples substituted with Bi while the *Staphylococcus aureus* bacterium has a higher sensitivity to pure hydroxyapatite. After 24 h of incubation, the antibacterial inhibition activity against *Escherichia coli* increases with increasing Bi concentration in hydroxyapatite, and the maximum antibacterial activity is observed for the HA-Bi-25 sample. On the other hand, an

Fig. 8. Microbial inhibition of the hydroxyapatite and Bi-substituted hydroxyapatite samples against *Escherichia coli* (a) and *Staphylococcus aureus* (b) bacteria (Color figure online).

increase in antibacterial activity for the Bi-substituted hydroxyapatite nanopowders is noticed for *Staphylococcus aureus*, but not as strong as for *Escherichia coli*. These results demonstrate that the Bi-substituted hydroxyapatite powders are more effective against Gram-negative bacteria than Gram-positive bacteria. The antibacterial property against *Escherichia coli* is improved after Ca<sup>2+</sup> substitution with Bi<sup>3+</sup> in the hydroxyapatite structure. This may be due to the greater solubility of Bi-substituted hydroxyapatite than that of pure hydroxyapatite, and more Bi ions are released to inhibit the existence of the tested bacteria as Bi increases in the hydroxyapatite. Also, the higher antibacterial inhibition activity against Gram-negative bacterial strains for Bi-substituted hydroxyapatite samples reveals that the increase in the Bi concentration may induce the positive surface charge for the apatite nanoparticles.

Taking into account the results obtained, it can be said that Bi-substituted hydroxyapatite nanopowders can be a promising antimicrobial agent due to their bioactive properties especially against Gram-negative bacteria.

Finally, the full characterization of these biomaterials would require the assessment of the bioactivity (by estimating their ability to stimulate the deposition of hydroxyapatite on their surface) and



biocompatibility (by testing cell proliferation and survival).

### CONCLUSION

The experimental results revealed that the Bi-substituted hydroxyapatite nanopowders,  $\text{Ca}_{10-x}\text{Bi}_x(\text{PO}_4)_6(\text{OH})_2$  where  $x = 0\text{--}2.5$ , were produced by the co-precipitation method using  $\text{Ca}(\text{OH})_2$ ,  $\text{H}_3\text{PO}_4$  and  $\text{Bi}(\text{NO}_3)_3 \cdot 5\text{H}_2\text{O}$  raw materials, as calcium, phosphorous and bismuth sources. The Bi content ranged between 5 and 25%. The XPS analysis of the doped samples indicated the presence of Bi in the apatite lattice as  $\text{Bi}^{3+}$ . The XRD results indicate that the Bi substitution did not change the crystal structures. The Bi-substituted hydroxyapatite particles have mesoporous textures with pore size in the range of 1.54–2.18 nm and specific surface area in the range of 12–24.86  $\text{m}^2/\text{g}$ . The typical yellow color was obtained after samples were calcined to 800°C. The final products were composed of spherical aggregates formed by nanoparticles with a size of about 30–55 nm. Due to the increase in the Bi content, the crystallites become smaller and form agglomerates owing to the size effect. In addition, their crystallinity decreases. The FTIR spectra show that Bi ions incorporated into the hydroxyapatite lattice reduce the acidity of the surface P-OH groups. The Bi-substituted hydroxyapatite powders are more effective against *Escherichia coli* Gram-negative bacterium than against *Staphylococcus aureus* Gram-positive bacterium.

### REFERENCES

1. F.C.M. Driessens and B. Soc, *Chim. Belg.* 89, 663 (1997).
2. M.T. Bernards, C. Qin, and S. Jiang, *Colloid Surf. B* 64, 236 (2008).
3. R.Z. LeGeros, *Clin. Orthop. Relat. R* 395, 81 (2002).
4. J.C. Elliott, *Structure and Chemistry of the Apatites and Other Calcium Orthophosphates* (Amsterdam: Elsevier Press, 1994), p. 111.
5. T. Tamm and M. Peld, *J. Solid State Chem.* 179, 1581 (2006).
6. J. Shepherd, D. Shepherd, and S. Best, *J. Mater. Sci.* 23, 2335 (2012).
7. S.Y. Lee, J.H. Kwak, M.S. Kim, S.W. Nam, T.H. Lim, S.A. Hong, and K.J. Yoon, *Korean J. Chem. Eng.* 24, 226 (2007).
8. K. Zhu, K. Yanagisawa, R. Shimanouchi, A. Onda, and K. Kajiyoshi, *J. Eur. Ceram. Soc.* 26, 509 (2006).
9. S.H. Lee and K.J. Yoon, *Korean J. Chem. Eng.* 18, 228 (2001).
10. I.R. de Lima, G.G. Alves, C.A. Soriano, A.P. Campanelli, T.H. Gasparoto, E.S. Ramos, L.A. de Sena, A.M. Rossi, and J.M. Granjeiro, *J. Biomed. Mater. Res. A* 98A, 351 (2011).
11. T.N. Kim, Q.L. Feng, J.O. Kim, J. Wu, H. Wang, G.Q. Chen, and F.Z. Cui, *J. Mater. Sci.* 9, 129 (1998).
12. B.J. Marshall, *Am. J. Gastroenterol.* 86, 16 (1991).
13. N. Yang and H. Sun, *Coord. Chem. Rev.* 251, 2354 (2007).
14. M. Stoltenberg, S. Juhl, and G. Danscher, *Eur. J. Histochem.* 51, 53 (2007).
15. L. Miersch, T. Rüffer, H. Lang, S. Schulze, M. Hietschold, D. Zahn, and M. Mehring, *Eur. J. Inorg. Chem.* 30, 4763 (2010).
16. F. Chen, C. Liu, and Y. Mao, *Acta Biomater.* 6, 3199 (2010).
17. A.W. Bauer, W.M. Kirby, J.C. Sherris, and M. Truck, *Am. J. Clin. Pathol.* 45, 493 (1966).
18. T. Suzuki, T. Hatsushika, and M. Miyake, *J. Chem. Soc. Farad. T.* 1, 3605 (1982).
19. H. Kim, R.P. Camata, Y.K. Vohra, and W.R. Lacefield, *J. Mater. Sci. Mater. Med.* 16, 961 (2005).
20. D.G. Guo, A.H. Wang, Y. Han, and K.W. Xu, *Acta Biomater.* 5, 3512 (2009).
21. E.I. Getman, A.V. Ignatov, S.N. Loboda, M.A.B.A. Jabar, A.O. Zhigailo, and A.S. Gluhova, *Funct. Mater.* 18, 293 (2011).
22. R.D. Shannon, *Acta Crystallogr. A* 32, 751 (1976).
23. A. Baumer, R. Caruba, H. Bizouard, and A. Peckett, *Can. Mineral.* 21, 567 (1983).
24. D. Bernache-Assollant, A. Ababou, E. Champion, and M. Heughebaert, *J. Eur. Ceram. Soc.* 23, 229 (2003).
25. R.J. Chung, M.F. Hsieh, R.N. Panda, and T.S. Chin, *Surf. Coat. Tech.* 165, 194 (2003).
26. M. Pourbaghi-Masouleh and H. Asgharzadeh, *Mater. Sci.—Pol.* 31, 424 (2013).
27. A. Serret, M.V. Cabanas, and M. Vallet-Regi, *Chem. Mater.* 12, 3836 (2000).